Propagation of Normal Zone in Quenching Superconducting Solenoids. Modeling Using COMSOL.

I. Terechkine

Introduction

To prevent irreversible damage of mechanical (e.g. high mechanical stress developed due to temperature gradients) or electrical (e.g. electric breakdown due to voltage generated in the system) origin in a quenching superconducting magnet from happening, propagation of normal zone must be well understood. For superconducting focusing lenses designed for HINS and PXIE projects, this type of a study was conducted using MATLAB environment. This approach seems straightforward and quite reliable as it allows simultaneous iterative solving of equations describing heat propagation in quenching system and evolution of electrical parameters of current discharge circuits (see references [1] to [6] for details). On the other hand, it requires significant preliminary work to find matrixes of magnetic field and mutual inductances of the system that usually comprise of several windings. If non-linear effects are significant, e.g. when ferromagnetic materials are used, multi-dimensional matrixes must be built and used to properly calculate the magnetic field within the system at any current by using multi-dimensional interpolation. Besides, each specific configuration of quench protection circuit requires some modification of a way how the currents in the system are calculated.

Main motivation for additional study in this field is to generalize the approach to this kind of modeling by using features of the latest versions of COMSOL multiphysics modeling tool that include multi-turn coil and electric circuit interfaces . As a result, it became possible to rely on automatic calculation of magnetic field and mutual inductances, even if non-linear effects are taken into account.

The final goal of this study is to confirm results obtained in [6] for the SSR1 lens of PXIE cryomodule using different modeling environment and to build a framework for studying more complicated systems. The first step made towards this goal must be validation of this new way to model QP in superconducting magnets. This validation is the subject of this note, and it is made by employing two different approaches to model quench propagation (both implemented in the COMSOL environment). The first way to set the model was by using the heat propagation module, AC/DC module's magnetic field node with the external current density, and the differential equation interface describing the loss of the magnetic energy in the resistive (after quench start) winding. The second approach utilized the heat propagation module, the multi-turn option of the magnetic field node, and the electric circuit interface. To simplify comparison of results, both approached were applied to a simple system containing only one coil. Only the second approach can be used for the analysis of the real multi-coil system analyzed in [6].

Coil Geometry

In both cases, the geometry of the main coil in [6] is used; it is implemented in 2D with axial symmetry. The length of the coil L = 111 mm, the inner diameter ID = 40 mm, and the outer diameter OD = 82 mm (so ΔR = 21 mm). There is 0.5 mm thick G-10 insulation applied to all outer surfaces of the coil. To solve the magnetic problem, the coil is placed in the center of a 100 mm radius and 200 mm height bounding cylinder. To help resolving voltages generated inside the coil during quenching, it was built of seven sections, each 3 mm thick (Fig. 1).

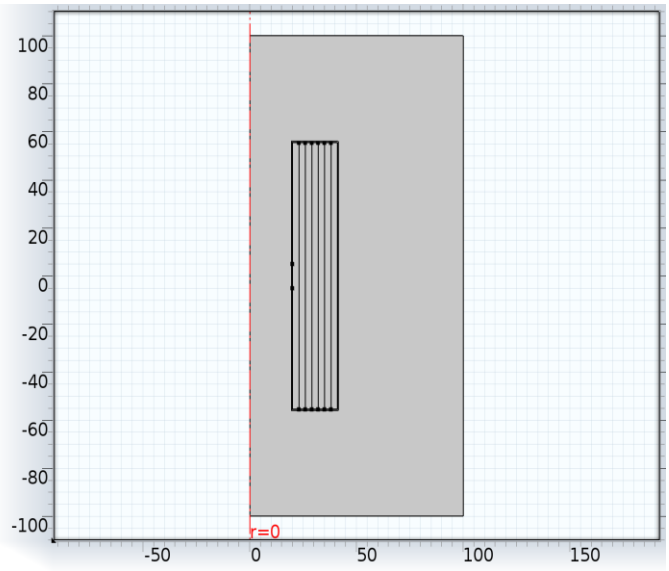

Fig. 1. Coil geometry

The coil is wound using 0.4 mm diameter NbTi 54/40 strand with copper to non-copper ratio of ~1.35 (Oxford Instruments). The number of turns in each layer N_t = 259 and the number of layers in the coil N_l = 48, making the total number of turns N_{tot} = 12432.

Heat transfer to liquid Helium bath is taken into account by employing temperature-dependent heat transfer coefficient.

Material properties: thermal conductivity and specific heat

As the system is at 2 K before quench and can warm up to room temperature, all physical properties of used materials must be described in the temperature range between 2 K and 300 K. Materials that were used to build the coil include NbTi and Cu as components of the strand and G10-type composite as the bonding material inside the coil and insulating material outside. Structure of the assembled coil can also be treated as a composite material which properties depend of the density of the winding (that is, mainly, on thickness of G10 insulation between the layers of winding in the coil).

The main component of the coil is 0.4 mm NbTi strand. Fig. 2 shows cross-section of the strand, where NbTi filaments (red) are embedded in copper matrix (grey).

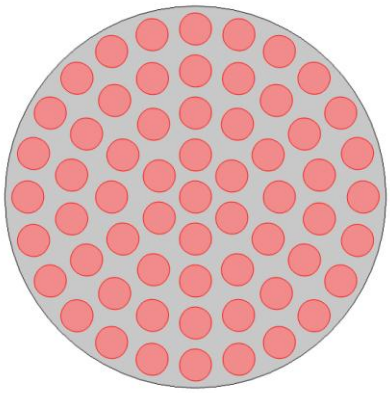

Fig. 2. Cross-section of NbTi strand.

Thermal conductivity and specific heat of basic materials in the coil structure are shown in figures 3 to 5 below.

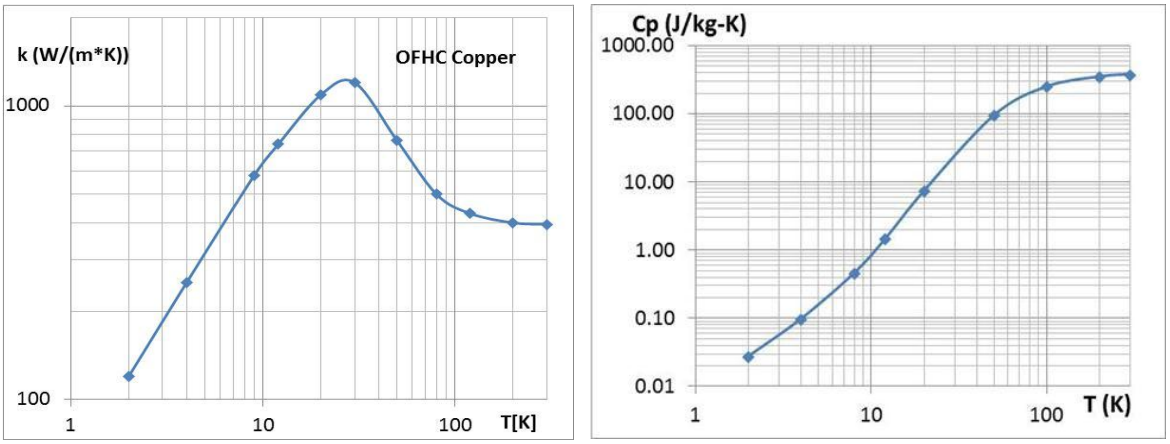

a) b)

Fig. 3. Heat conductivity (a) and specific heat (b) of OFHC copper with RRR = 100 [7].

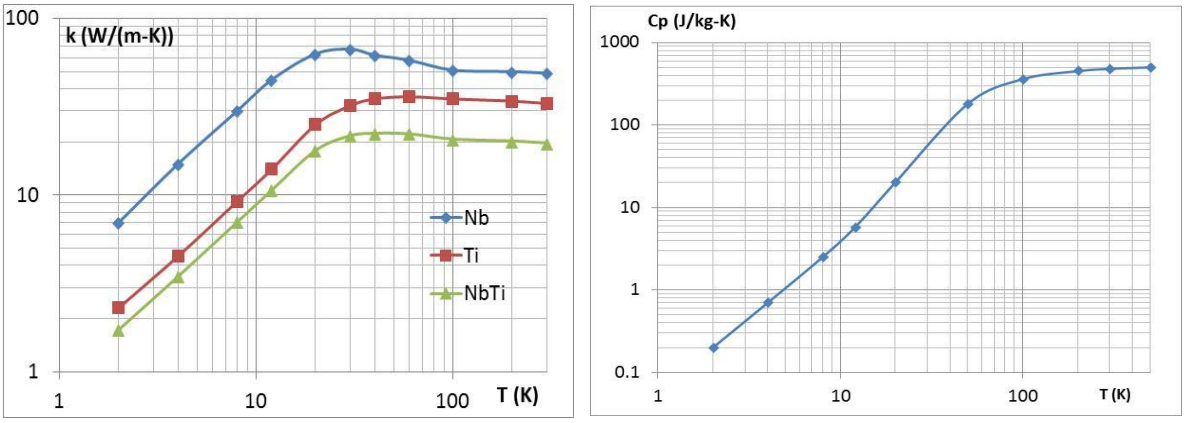

a) b)

Fig. 4. Heat conductivity (a) and specific heat (b) of NbTi [8].

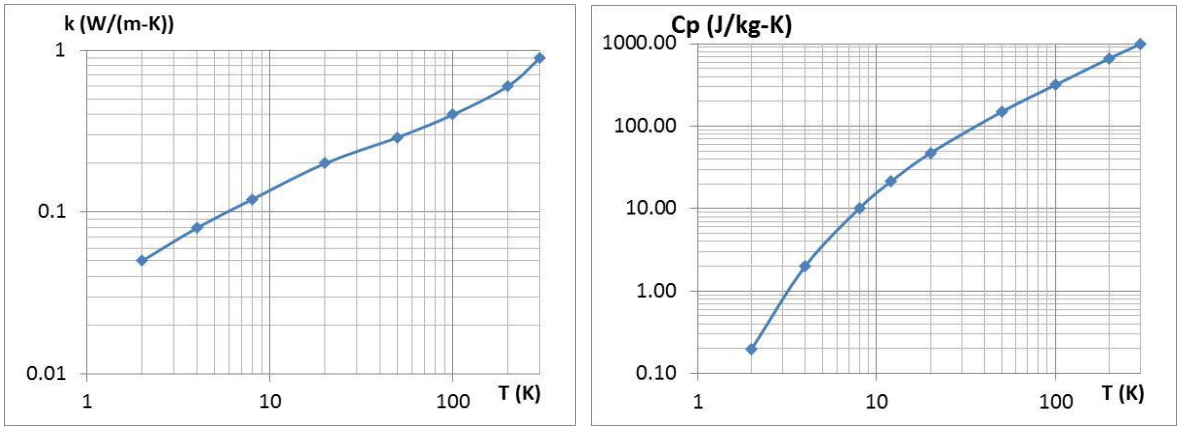

a) b)

Fig. 5. Heat conductivity (a) and specific heat (b) of G-10 material [7].

Small (~2 x 2 mm^2) cut-off from the cross-section of epoxy-impregnated coil wound using regular pattern is shown in Fig. 6.

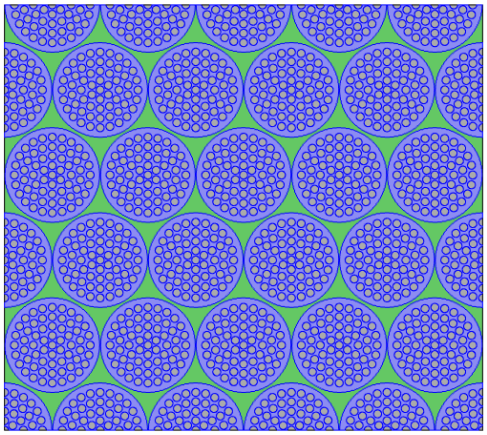

Fig. 6. Regular winding pattern of a superconducting coil

In each layer, the winding is relatively tight, but in the radial direction the density of winding depends on the amount of the interlayer insulation. Quantitatively, the density of winding is described as a ratio of the cross-section area occupied by the strands to the total cross-section area of the coil. Winding density corresponding to the cross-section in Fig. 6 is relatively high (0.86); the advantage of having higher winding density is getting higher thermal conductivity in the radial direction that results in better spread of the heat generated during quenching.

Knowing winding pattern, it is straightforward to find radial and longitudinal thermal conductivity of the coil structure and the average specific heat. Tables 1 and 2 below were generated by solving heat transfer problems in the longitudinal and the radial directions for windings with different winding densities α. Corresponding graphs are shown in Fig. 7; one can see that the properties of the coil are anisotropic.

Table 1. Thermal conductivity of a coil composite in the longitudinal direction.

T (K)	α = 0.864	α = 0.778	α = 0.707	α = 0.648	α = 0.598	α = 0.555
2	1.54	1.24	1.11	1.01	0.94	0.87
4	2.29	1.84	1.64	1.50	1.39	1.30
8	3.32	2.66	2.38	2.18	2.02	1.88
12	4.14	3.32	2.97	2.72	2.51	2.34
20	5.44	4.36	3.90	3.57	3.30	3.07
30	6.53	5.23	4.68	4.28	3.96	3.69
50	7.69	6.18	5.52	5.05	4.67	4.36
75	8.94	7.19	6.43	5.89	5.45	5.08
100	10.25	8.26	7.39	6.76	6.26	5.83
200	14.73	11.94	10.69	9.78	9.05	8.44
300	20.87	17.04	15.25	13.97	12.93	12.05

Table 2. Thermal conductivity of a coil composite in the radial direction.

T (K)	α = 0.864	α = 0.778	α = 0.707	α = 0.648	α = 0.598	α = 0.555
2	0.92	0.40	0.27	0.21	0.18	0.16
4	1.36	0.59	0.40	0.31	0.26	0.23
8	1.97	0.85	0.58	0.45	0.38	0.33
12	2.46	1.06	0.72	0.56	0.47	0.42
20	3.22	1.39	0.95	0.74	0.62	0.54
30	3.87	1.67	1.14	0.89	0.75	0.65
50	4.60	1.99	1.36	1.06	0.89	0.78
75	5.40	2.35	1.60	1.26	1.06	0.93
100	6.23	2.72	1.86	1.46	1.23	1.08
200	9.14	4.04	2.77	2.18	1.83	1.61
300	13.30	5.98	4.13	3.25	2.74	2.40

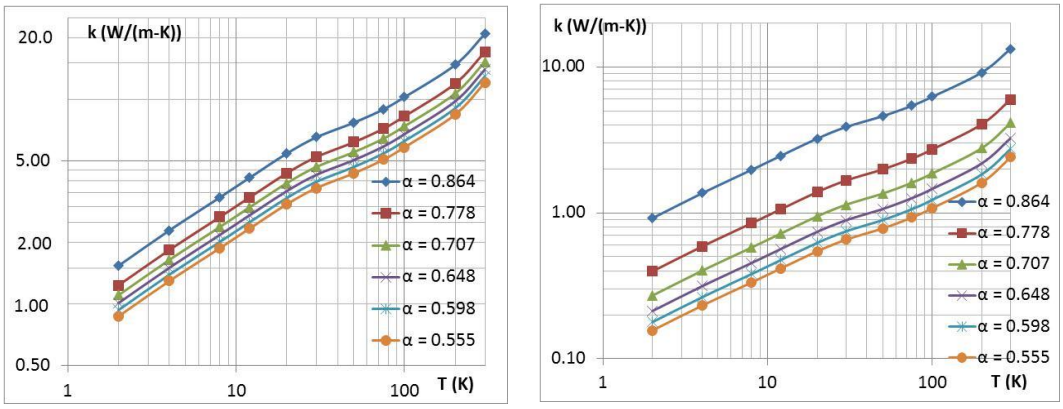

a) b)

Fig. 7. Longitudinal (a) and radial (b) thermal conductivity of wound coil structure for different values of winding density α.

To find average specific heat of the winding, we need to take into the account both the copper-to-non-copper ratio ***k*** and the winding density factor ***α***. As both of the factors refer to the surface area occupied by the constituents in the cross-section of the coil, it is appropriate to use the volumetric heat capacity $C_V = \mathbf{\rho \cdot C_P}$ of each material to find the effective volumetric heat capacitance of the winding composite.

$$C_{V\_eff} = \rho_{G10}\cdot(1-\alpha)\cdot C_{P\text{-}G10} + \rho_{Cu}\cdot\alpha\cdot k/(1+k)\cdot C_{P\text{-}Cu} + \rho_{NbTi}\cdot\alpha\cdot 1/(1+k)\cdot C_{P\text{-}NbTi} \qquad /1/$$

Then, specific heat of the winding can be found as

$$C_{P\_eff} = C_{V\_eff} / \rho_{eff}$$

with

$$\rho_{eff} = \rho_{G10}\cdot(1-\alpha) + \rho_{Cu}\cdot\alpha\cdot k/(1+k) + \rho_{NbTi}\cdot\alpha\cdot 1/(1+k) \qquad /2/$$

Having ρ_{Cu} = 9000 kg /m^3 (at 4 K), ρ_{NbTi} = 6000 kg/m^3, and ρ_{G10} = 1800 kg/m^3, and knowing the values of Cp for copper, NbTi, and G-10, we can calculate the values of $\mathbf{C_{P\_eff}}$ for the windings with different densities of winding. Table 3 below summarizes results of this calculation assuming k = 1.35 for the chosen strand.

Table 3. Specific weight (kg/m^3) and specific heat of windings (J/(kg·K)) with different densities winding α in the temperature range from 2 K to 300 K

α	ρ (kg/m^3)	2 K	4 K	8 K	12 K	20 K	50 K	100 K	200 K	300 K
0.864	6904	0.090	0.36	1.46	3.54	12.9	125	290	397	437
0.778	6396	0.093	0.41	1.70	4.03	13.9	126	291	404	453
0.707	5976	0.096	0.45	1.93	4.51	14.8	126	292	411	468
0.648	5628	0.098	0.49	2.15	4.95	15.7	127	292	418	482
0.598	5332	0.101	0.53	2.35	5.37	16.5	127	293	425	495
0.555	5078	0.103	0.57	2.55	5.78	17.3	128	294	431	508

The values of specific heat for different winding densities are also shown in Fig. 8.

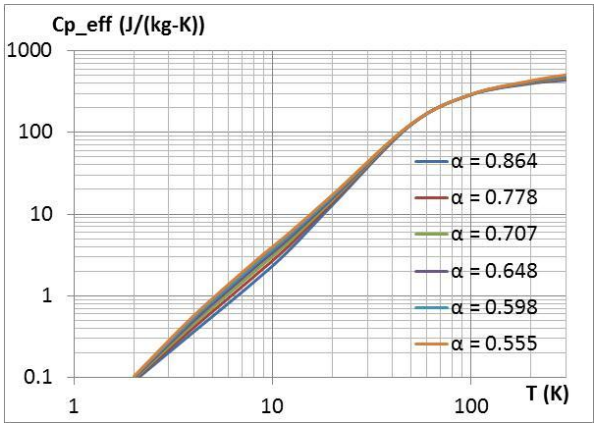

Fig. 8. Specific heat of epoxy-impregnated windings with different densities.

In this study, specific heat corresponding to the filling factor of the SSR1 lens (α = 0.687) will be used; it is found using interpolation and is shown in Fig. 9 together with the similar data for the constituting materials.

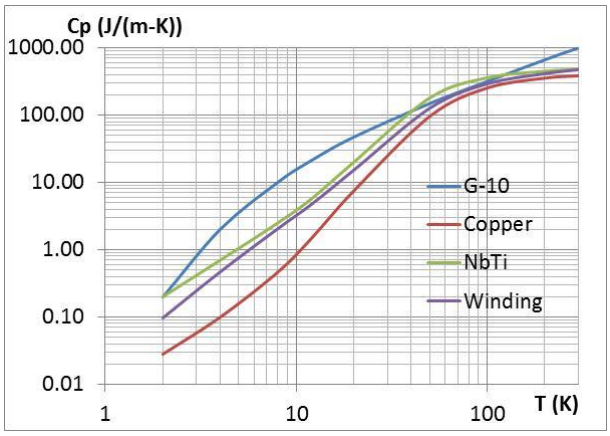

Fig. 9. Specific heat of the SSR1 coil winding in comparison with that of the constituents.

Material properties: critical surface of the strand

Parameterization of the critical surface will be implemented following the approach described in [9]. The next set of dimensionless parameters is used:

$t = T/T_{c0}$, where T_{c0} **= 9.35 K** is the maximum critical temperature (at B = 0).

$b = B/B_{c2}(T)$,where $B_{c2}(T)$ is the upper critical field of NbTi:

$$B_{c2}(T) = B_{c20}\cdot(1-t^n) \qquad /3/$$

where B_{c20} **= 14.25 K** is the maximum upper critical field (at T **= 0**) and n = 1.7.

The ratio of the maximum current density in the superconductor at any magnetic field and temperature to that at B = 5 T and T = 4.2 K can be found using the next expression:

$$J_c(B,T) / J_c(5\text{ T}, 4.2\text{ K}) = C_0/B\cdot b^{\alpha}\cdot(1-b)^{\beta}\cdot(1-t^n)^{\gamma} \qquad /4/$$

where C_0 = 28.4 T, α = 0.80, β = 0.89, and γ = 1.87.

For the NbTi Oxford 54-filament (54/40) 0.4 mm (k = 1.35) conductor, the value of critical current corresponding to the 4.2 K temperature and 5 T magnetic field I_c(4.2K, 5T) = 140 A in accordance with the vendor's specification [10]. This gives the reference current density in the superconductor

$J_c(4.2K, 5T) = I_c(4.2K, 5T) / S_{s/c} = (1 +k)\cdot I_c(4.2K, 5T) / S_w = 2.35\cdot 140/0.12566 \approx$ **2600 A/mm^2**.

Fig. 10 (a and b) shows graphs of the relative critical current density $J_c(T,B) / J_c$(4.2K, 5T,) as a function of temperature T using magnetic field B as a parameter (a) and as a function of the magnetic field B using temperature T as a parameter (b). These graphs are obtained by sectioning the critical surface by the planes B = const (a) and T = const (b).

After the critical surface is defined, the critical current density can be readily found for the 0.4 mm wire at any field and at any temperature. Table 4 below contains this information.

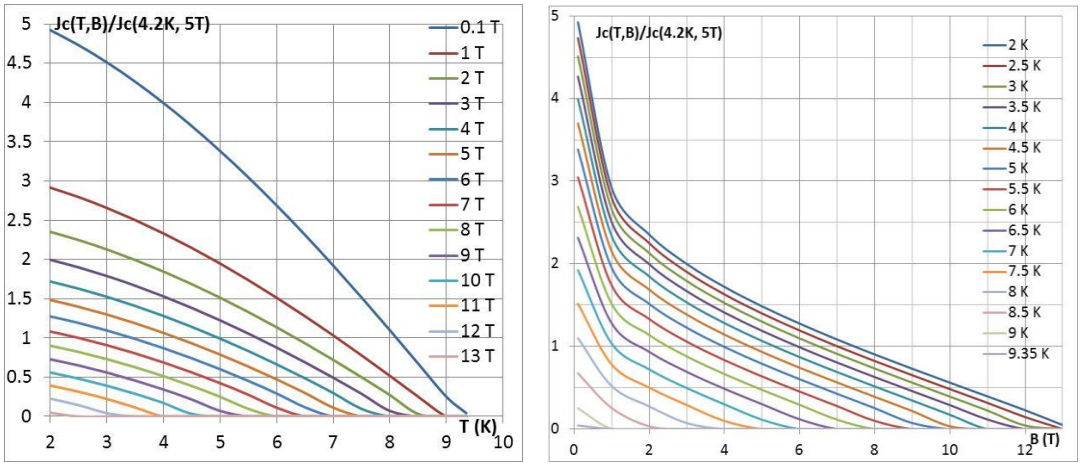

a) b)

Fig. 10. Projections of the critical surface of NbTi on the planes B = const (a) and T = const (b).

Table 4. Critical current of 0.4 mm NbTi strand as a function of magnetic field and temperature.

T(K) \ B (T)	0.1 T	1 T	2 T	3 T	4 T	5 T	6 T	7 T	8 T	9 T	10 T	11 T	12 T	13 T
2	688.96	408.05	329.23	279.37	240.64	207.77	178.47	151.53	126.21	101.99	78.47	55.26	31.82	6.69
2.5	662.18	391.21	314.62	265.94	227.98	195.68	166.80	140.19	115.10	91.03	67.55	44.22	20.26	0.00
3	631.43	371.89	297.86	250.53	213.47	181.80	153.41	127.15	102.31	78.38	54.89	31.26	5.93	0.00
3.5	596.99	350.25	279.10	233.28	197.20	166.25	138.39	112.51	87.93	64.09	40.46	16.09	0.00	0.00
4	559.07	326.43	258.44	214.28	179.30	149.12	121.82	96.34	71.98	48.14	24.05	0.00	0.00	0.00
4.5	517.86	300.55	236.00	193.66	159.85	130.50	103.79	78.68	54.46	30.36	4.58	0.00	0.00	0.00
5	473.56	272.73	211.89	171.49	138.94	110.45	84.32	59.52	35.22	10.01	0.00	0.00	0.00	0.00
5.5	426.35	243.10	186.21	147.87	116.64	89.03	63.42	38.73	13.64	0.00	0.00	0.00	0.00	0.00
6	376.40	211.77	159.07	122.89	93.01	66.24	40.98	15.75	0.00	0.00	0.00	0.00	0.00	0.00
6.5	323.92	178.87	130.57	96.64	68.10	42.00	16.43	0.00	0.00	0.00	0.00	0.00	0.00	0.00
7	269.14	144.56	100.84	69.19	41.83	15.71	0.00	0.00	0.00	0.00	0.00	0.00	0.00	0.00
7.5	212.33	109.02	70.02	40.52	13.58	0.00	0.00	0.00	0.00	0.00	0.00	0.00	0.00	0.00
8	153.87	72.51	38.19	9.94	0.00	0.00	0.00	0.00	0.00	0.00	0.00	0.00	0.00	0.00
8.5	94.35	35.36	4.53	0.00	0.00	0.00	0.00	0.00	0.00	0.00	0.00	0.00	0.00	0.00
9	35.01	0.00	0.00	0.00	0.00	0.00	0.00	0.00	0.00	0.00	0.00	0.00	0.00	0.00
9.35	5.95	0.00	0.00	0.00	0.00	0.00	0.00	0.00	0.00	0.00	0.00	0.00	0.00	0.00

Material properties: specific resistance of copper

During quenching, superconducting strand turns normally conducting, and its resistance (and corresponding energy loss) is defined by properties of copper used as a matrix. RRR of copper used for strand production is usually within the range from 50 to 150. We will use the value RRR=100 in this study. Resistivity of copper depends on the temperature and the magnetic field:

$$\boldsymbol{\rho_{Cu}(T,B) = \rho_{Cu}(T,0) + \rho_m(B)} \qquad /5/$$

The magneto-resistivity of copper $\boldsymbol{\rho_m(B)}$ can be evaluated using the Kohler rule [11]:

$$\boldsymbol{\rho_m}\ (\text{Ohm}\cdot\text{m}) = \boldsymbol{a \cdot B}\ (\text{T}) \qquad /6/$$

with $\mathbf{a} = 4.5\cdot10^{-11}$ Ohm·m/T.

Using this rule for copper with RRR = 100, we can find values of resistivity in the range of temperatures and magnetic fields, like shown in Table 5 below. The data in the table is illustrated by the graphs in Fig. 11.

Table 5. Resistivity of RRR 100 copper for different temperatures and magnetic field levels.

T (K)	2	4	8	12	20	50	100	200	300
0 T	1.60E-10	1.60E-10	1.60E-10	1.62E-10	1.90E-10	6.00E-10	4.00E-09	1.10E-08	1.70E-08
1 T	2.05E-10	2.05E-10	2.05E-10	2.07E-10	2.35E-10	6.45E-10	4.05E-09	1.10E-08	1.70E-08
2 T	2.50E-10	2.50E-10	2.50E-10	2.52E-10	2.80E-10	6.90E-10	4.09E-09	1.11E-08	1.71E-08
3 T	2.95E-10	2.95E-10	2.95E-10	2.97E-10	3.25E-10	7.35E-10	4.14E-09	1.11E-08	1.71E-08
4 T	3.40E-10	3.40E-10	3.40E-10	3.42E-10	3.70E-10	7.80E-10	4.18E-09	1.12E-08	1.72E-08
5 T	3.85E-10	3.85E-10	3.85E-10	3.87E-10	4.15E-10	8.25E-10	4.23E-09	1.12E-08	1.72E-08
6 T	4.30E-10	4.30E-10	4.30E-10	4.32E-10	4.60E-10	8.70E-10	4.27E-09	1.13E-08	1.73E-08

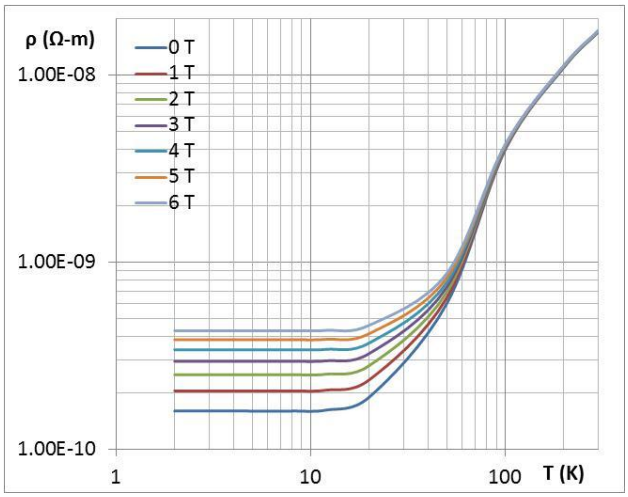

Fig. 11. Resistivity of RRR 100 copper as a function of temperature for different levels of magnetic field.

The data in Table 5 can be reasonably well approximated by the analytical expression that includes a logical term (T > 43 K):

$$\rho(\boldsymbol{T},\boldsymbol{B}) = 1.6\cdot10^{-10} + 6.7\cdot10^{-11}\cdot(\boldsymbol{T}\text{-}43[\text{K}])\cdot(\boldsymbol{T}[1/\text{K}]>43)+4.5\text{E-}11\cdot\boldsymbol{B} \qquad /7/$$

Fig. 12 compares the values of the resistivity obtained by using this expression (red diamonds) with those from the table for B = 0.

One needs to keep in mind that expression /7/ only works for copper in the strand. When the filaments in the strand are in the superconducting state, the resistive copper matrix is effectively shunted by zero resistance. To take this into account, /7/ is multiplied by a logical expression, which, at any specific location within the coil, takes the unit value when the current in the winding becomes higher than the critical current defined by the expression similar to that in /4/:

$$I > Icr = Icr|_{4.2K,5T}\cdot\mathbf{C_0}/\boldsymbol{B}\cdot\mathbf{b}^{\alpha}\cdot(\mathbf{1\text{-}b})^{\beta}\cdot(\mathbf{1\text{-}t}^{\mathbf{n}})^{\gamma} \qquad /8/$$

where $Icr|_{4.2K,5T}$ = 140 A in accordance with the data in Table 4.

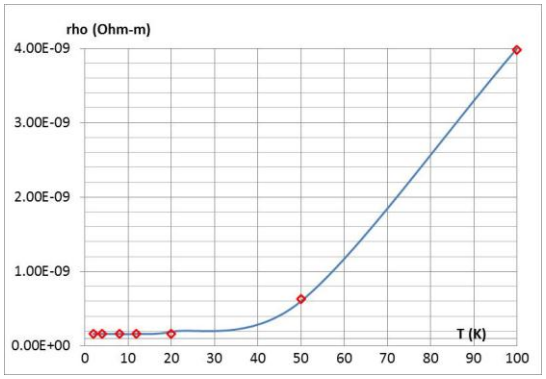

Fig. 12. Copper resistivity at B = 0 (blue curve) vs evaluated by using /7/ (red diamonds).

Material properties: heat transfer to liquid Helium

As was made in [12], heat transfer coefficient from the outer boundary of the assembly (electrically insulated by 0.5 mm thick layer of G-10) into LHe at 2 K is described by a temperature-dependent heat transfer coefficient K (W/(m^2·K):

$$K(\boldsymbol{T}) = 10\cdot\boldsymbol{T} + 6000/T \qquad /9/$$

Graph in Fig. 13 shows this coefficient in the temperature range from 2 K to 300 K. The low-temperature part of the graph is defined mainly by Kapitsa resistance; the curve goes though a minimum due to the onset of boiling and its progression from the nucleate stage to the film-boiling stage. The rise of the heat transfer coefficient after the minimum is due to the increase of the mass transfer part of the heat propagation, which, in turn, is due to the increased velocity of He gas near the heated surface.

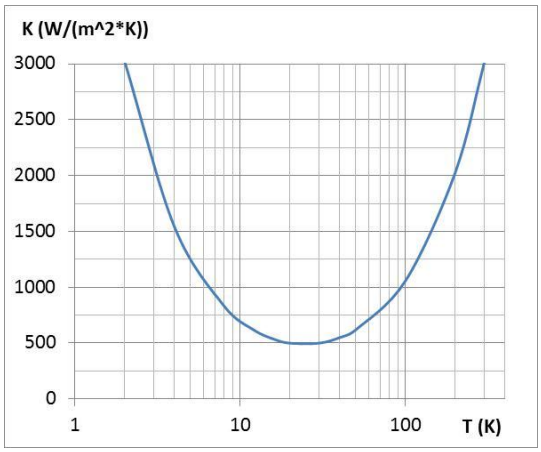

Fig. 13. Heat transfer coefficient to 2K LHe

Initiation of quench

In both cases of the study, coil quenching was initiated by using a pulsed heat source on the inner boundary of the coil (limited by two dots in Fig. 1). The amount of heat needed for quenching depends on the initial current. If the current is close to the achievable maximum, the total deposited heat of ~50 mJ reliably initiates the transition.

Propagation of the normal zone in superconducting magnets

If a small volume of a winding in a superconducting magnet turns normally conducting, it becomes a source of heat, which is generated by the current in the strand. This heat increases the temperature of the strand, and the temperature gradients lead to propagation of the heat through the winding resulting in an avalanche-type growth of the resistance. As a rule of thumb, after the occurrence of the quench is detected (usually the detection is based on the voltage generated in the winding), the power supply is phased out and the system is discharged. Besides the resistance of the coil, which is changing during quenching, the discharge circuit can have additional series resistance introduced to remove some energy out of the coil (e.g. see [3]). The coil can also be permanently connected to a parallel resistance serving the same purpose (see [5]). To find the current in the coil at each moment during the quench, specific configuration of the discharge circuit must be used and appropriate algorithm must be employed to resolve the circuit (or the energy balance) equations. The energy loss depends on the resistivity of copper, which is a function of the temperature and the magnetic field, so the magnetic field must be resolved for every part of the coil.

As a result, modeling of quench propagation in a superconducting magnet must be made by solving simultaneously for the heat propagation, for the magnetic field, and for the currents in the protection circuit. With the introduction of the circuit interface and the multi-turn coil interface in COMSOL, all needed tools for the modeling became available.

As an alternative way, for the simple coil in Fig. 1, the energy conservation law can be used to find the discharge current. This makes a good mean for verification of results obtained by using the circuit interface. For the heat propagation part of the problem, power density associated with the energy loss on the resistive elements of the winding can be found using the logic that starts from the basic expression for the power density: $P = I^2 \cdot R$. The resistance of small volume of the normally conducting part of the winding can be expressed as

$$dR = \rho(\boldsymbol{T}, \boldsymbol{B}) \cdot dl / S_{Cu} \qquad /10/$$

where dl is the total length of the strand within the analyzed elementary volume. Assuming the axial symmetry (which means that is in the azimuthal direction $\boldsymbol{T}$ and $\boldsymbol{B}$ do not change) the length of the strand dl in the volume of the interest is proportional to the number of turns dN in corresponding surface element $dS = dr \cdot dz$: $dN = N_t/L \cdot dz \cdot N_l/\Delta R \cdot dr$. As the length of the strand within the volume of interest is proportional to the radius,

$$dl = 2\pi \cdot r \cdot N_l/\Delta R \cdot dr \cdot N_t/L \cdot dz = 2\pi \cdot r \cdot N_{tot}/S_{coil} \cdot dS_{coil} \qquad /11/$$

with $S_{coil} = \Delta R \cdot L$. As a result,

$$dR = 2\pi \cdot N_{tot}/(S_{coil} \cdot S_{Cu}) \cdot r \cdot \rho(\boldsymbol{T}, \boldsymbol{B}) \cdot dS_{coil} \qquad /12/$$

or

$$dR = N_{tot}/(S_{coil} \cdot S_{Cu}) \cdot \rho(T,B) \cdot dV_{coil} \qquad /13/$$

So the density of the power loss can be written as

$$p = dP/dV = I^2 \cdot N_{tot}/(S_{coil} \cdot S_{Cu}) \cdot \rho_{Cu}(T,B) \qquad /14/$$

S_{Cu} can be expressed in terms of the strand cross-section and the Cu/nCu ratio k:

$$S_{cu} = k/(1+k) \cdot S_w$$

Having in mind the effective density of the winding in the coil $\alpha = N_{tot} \cdot S_w / S_{coil}$, S_w can be expressed in terms of the coil cross-section: $S_w = \alpha \cdot S_{coil}/N_{tot}$. As a result, the power density of the energy loss in the coil can be written as

$$p = (1+k)/(\alpha \cdot k) \cdot (N_{tot}/S_{coil})^2 \cdot I^2 \cdot \rho_{Cu}(T,B) = (1+k)/(\alpha \cdot k) \cdot J_{av}^2 \cdot \rho_{Cu}(T,B) \qquad /15/$$

where J_{av} is the average current density in the winding.
Expression /15/ will be used as a source power in the heat propagation part of the modeling.

To find the current during quench, let's first consider using a simple discharge circuit where the coil's resistance is the only element. In this case we can write down a differential equation that defines the change of the current in the system starting with the energy conservation law that states that the loss of the magnetic energy initially stored in the coil must be equal to the heat generated by the resistive heating:

$$dW/dt = -P = -(1+k)/(\alpha \cdot k) \cdot (N_{tot}/S_{coil})^2 \cdot I^2 \cdot \int \rho_{Cu}(T,B) \cdot dV_{coil}$$

Having in mind that $W = 1/2 \cdot L_{coil} \cdot I^2$,

$$dI/dt = -(1+k)/(\alpha \cdot k) \cdot I/ L_{coil} \cdot (N_{tot}/S_{coil})^2 \cdot \int \rho_{Cu}(T,B) \cdot dV_{coil} \qquad /16/$$

where L_{coil} is the inductance of the coil.

In the simplest case of a one-coil system, this equation replaces the need to use electrical circuit interface. Resistance of the quenching coil, or of any part of the coil, can be found by using the expression

$$R = (1+k)/(\alpha \cdot k) \cdot (N_{tot}/S_{coil})^2 \cdot \int \rho_{Cu}(T,B) \cdot dV, \qquad /17/$$

where the integration is performed in the volume of the coil's sub-sections in Fig. 1.

Mutual inductances in the coil

During quenching, significant electric field can be generated in the winding as there is the voltage drop on the resistance of normally conducting strand and the inductive voltage due to the change of the current. For the model under study, the coil was divided into several connected in series and inductively coupled sub-sections; required number of the sub-sections depends on the desired accuracy. In this study seven (7) sections were used with the same inner radius and different outer radii: it was increased by 3 mm steps. Assuming grounded inner layer of the coil, inductive voltage generated in each sub-section is the product of the current derivative and the mutual inductance between this particular sub-section and the total coil.

The mutual inductance $\boldsymbol{M_{ri}}$ between the whole coil and its part limited by the outer radius r_i can be found by using a magnetic solver and employing the expression

$$M_{ri} = \frac{1}{I} \times \frac{N}{S_{coil}} \times \int_{r0}^{ri} A_{phi}\, dV \qquad /18/$$

where A_{phi} is the vector-potential inside the sub-section corresponding to current $\boldsymbol{I}$ in the main coil, and the integral is taken over the area of the coil limited to the radius r_i. Corresponding data are shown in Table 6.

Table 6. Mutual inductances between the whole coil and the sub-coils limited by the outer radii r_i

r_i (mm)	0	3	6	9	12	15	18	21
M_{ri} (H)	0	0.2804	0.6326	1.0506	1.5250	2.0429	2.5877	3.1392

Obviously, the inductance of the coil is equal to the mutual inductance of the coil to itself: $L_{coil} \equiv M_{21}$.

It is necessary to mention here that the array of the mutual inductances is needed only if we use the equation-based method for solving the quench propagation problem. When the electric circuit interface and the multi-coil interface are used, the mutual inductances are calculated automatically.

Equation-based modeling of the quench propagation problem

If the initiating heater is off, the maximum current in the coil that does not break superconductivity at 2 K is 82.5 A; this corresponds to the value of the critical current found for the strand at 2 K using magnetic modeling means. The initial current in the circuit is set to 80 A; heat pulse of 50 mJ is used to initiate the quench.

Following is a description of main functions used during modeling. Dependence of the critical field on the temperature (see expression /3/) is shown in Fig. 14.

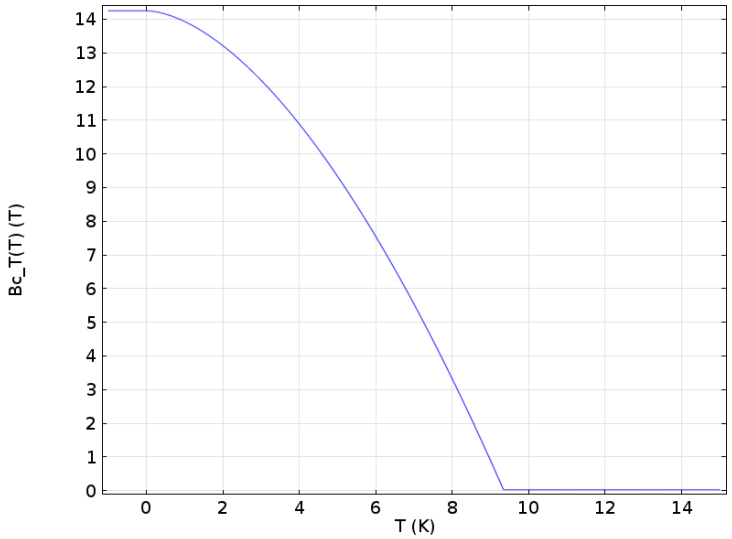

Fig. 14. Temperature-dependent critical field $B_{c2}(T)$

Fig. 15 shows graphical representation of the relative magnetic field, which is a function of the magnetic field and the temperature. When the temperature exceeds 9.35 K, or when magnetic field exceeds 14.25 T, b = 1. In all other cases, it is defined by the expression $b = B/B_{c2}(T)$.

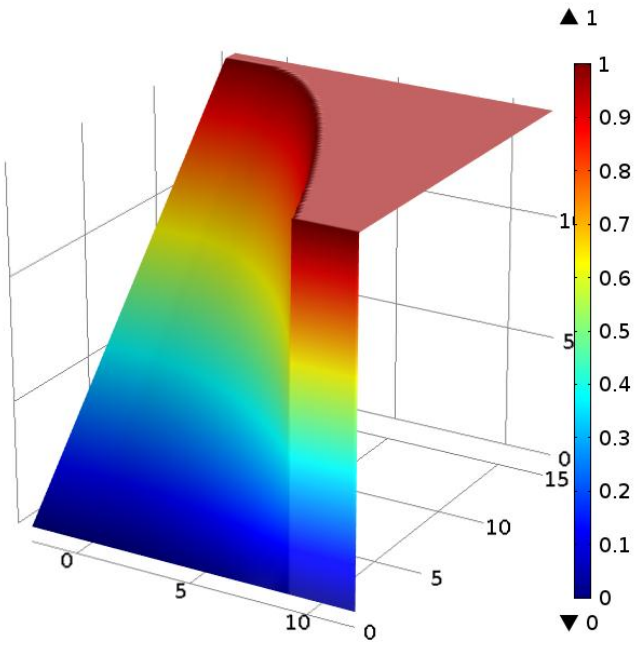

Fig. 15 Relative magnetic field b = $B/B_{c2}(T)$

The critical current is defined by the expression similar to that in /8/. The difference is that the magnetic field is modified by adding a small component ΔB = 1 mT to avoid the appearance of zero in the denominator.

$$Icr = Icr|_{4.2K,5T} \cdot C_0/(B+\Delta B)\cdot b^{\alpha}\cdot(1-b)^{\beta}\cdot(1-t^n)^{\gamma} \qquad /19/$$

Corresponding critical surface is shown in Fig. 16.

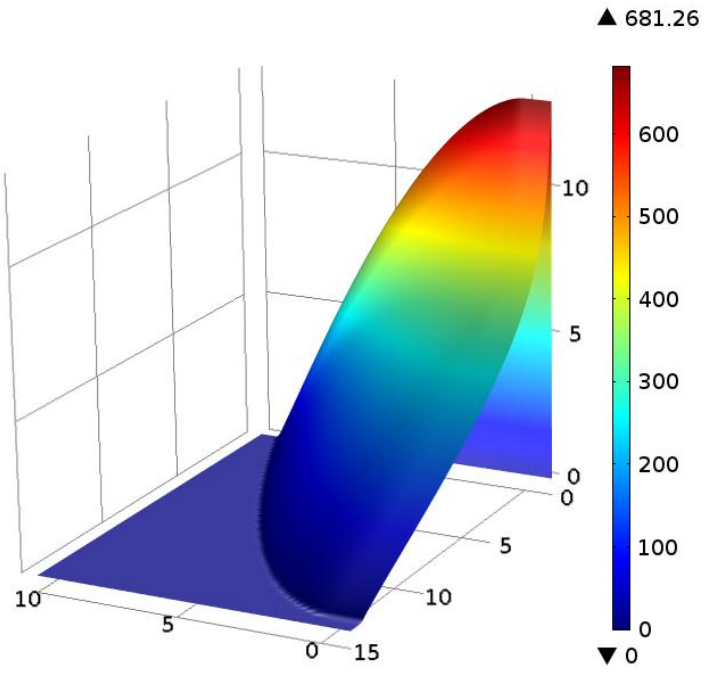

Fig. 16. Critical current of the strand.

Main results of the modeling using the equation-based approach are summarized in figures below. The plot of the current and current derivative is in Fig. 17.

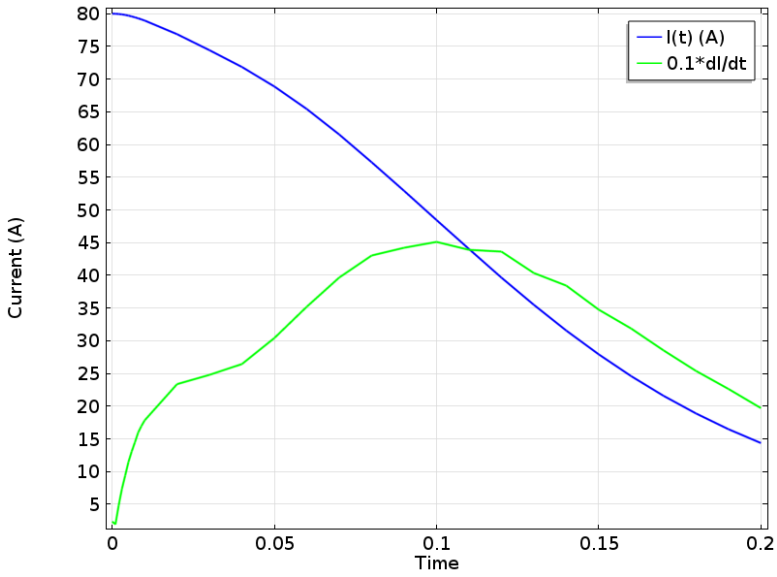

Fig. 17. Current and current derivative

Fig. 18 shows the maximum and the average temperature within the winding as well as the temperature at the point of the maximum field: r = 20 mm, z = 0. This temperature is lower than the maximum one because of the cooling by LHe.

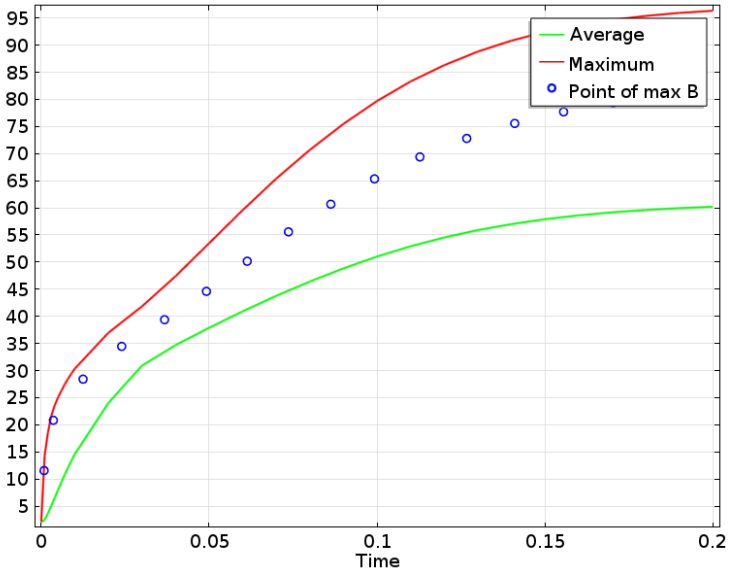

Fig. 18. Temperature inside the coil

Coil resistance vs time is plotted in Fig. 19.

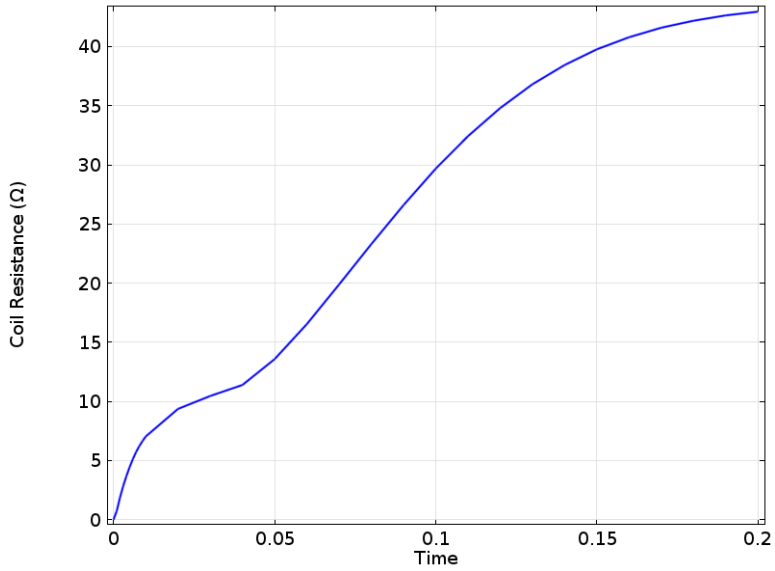

Fig. 19. Coil resistance

Heating power is found by using the expression $P = I^2 \cdot R$. It reaches the maximum of 75 kW at the moment t = 80 ms. Corresponding graph is in Fig. 20. Integrating this curve, we get the total energy deposited in the coil of ~9.9 kJ, which corresponds to the energy initially stored in the system.

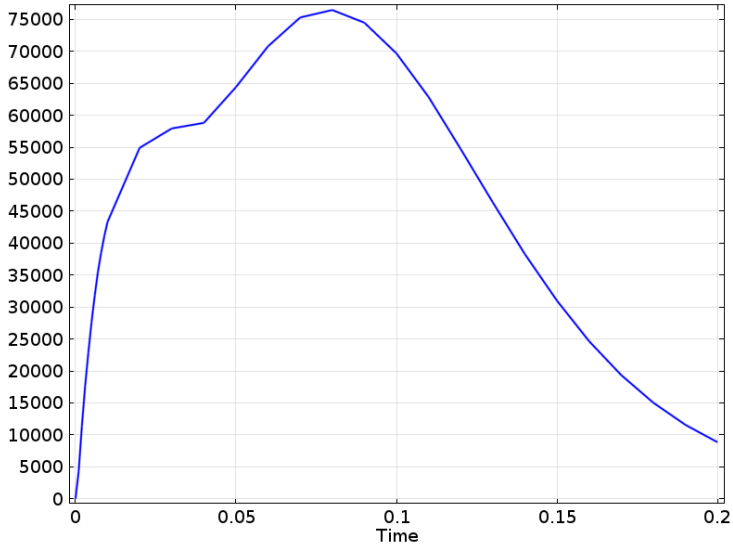

Fig. 20. Heating power $P = I^2 \cdot R$

Fig. 21 compares the resistive and the inductive voltage in the coil. Because we do not have any external resistance in the discharge circuit, the total voltage difference must be zero at any moment of time, so the two curves must coincide, which we can indeed observe.

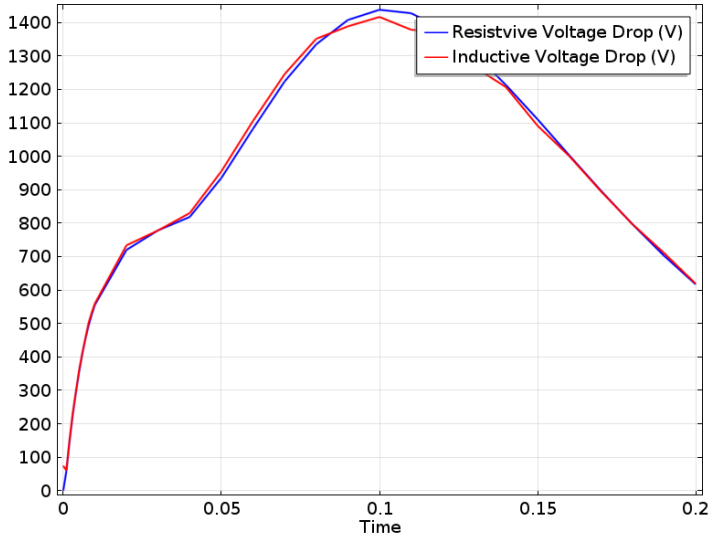

Fig. 21. Resistive and inductive voltage generated on the ends of the coil

Fig. 22 shows how layer voltages (relative to the inner layer) change in time. The maximum voltage is observed between the layers with radii between 9 mm and 12 mm.

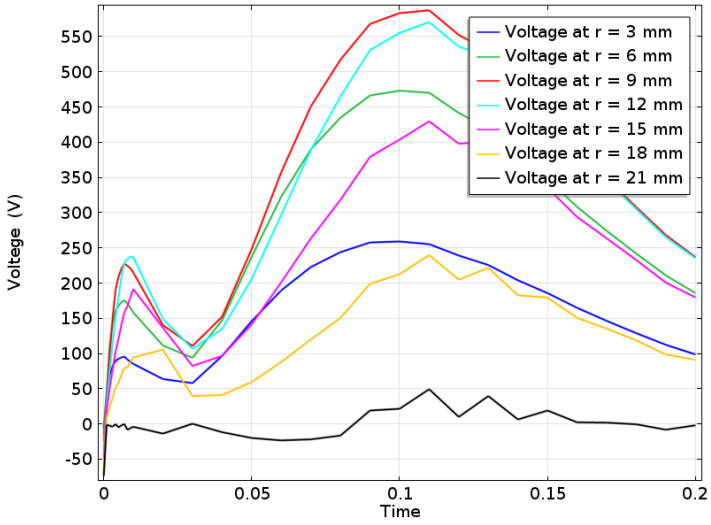

Fig. 22. Voltages inside the coil relative to the inner layer (r = 0)

Finally, in Fig. 23 one can see the voltage inside the winding at different moments of time. The distance from the inner layer is a parameter here. This is just another way to visualize information already shown in Fig. 22. The maximum voltage of ~600 V is reached in 100 ms in the middle of the coil. At $\Delta r = 21$ mm, the voltage must be zero by definition; some remaining voltage that one see in Fig. 23 at this point tells about the precision of the modeling.

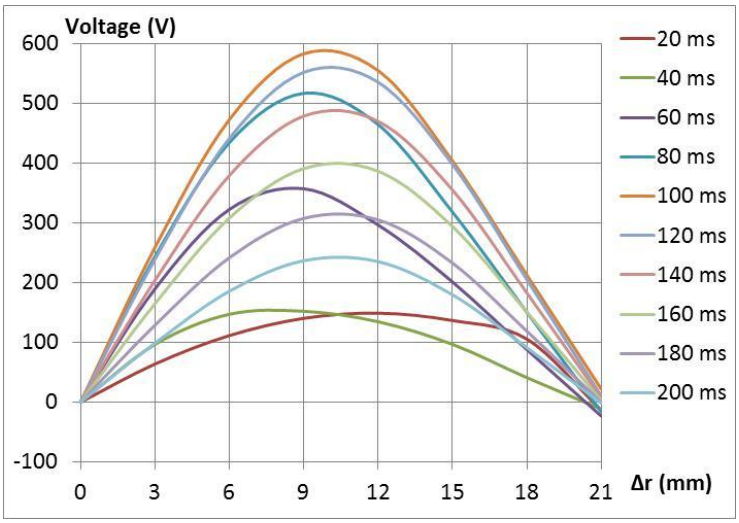

Fig. 23. Voltage to the ground generated in the winding during quenching.

Circuit-based modeling of the quench propagation problem

Geometry of the system in this case remains as shown in Fig. 1. Seven sub-sections of the coil, each 3 mm thick, are introduced; all sub-sections are connected in series using the "circuit" interface of COMSOL. Voltage supply generates voltage pulse that brings the current to a desired level (in this particular case it is 80 A). As the current reaches his level, the heater starts acting, inducing quench. Fig. 24 shows the source voltage, the current in the circuit, and the timing of the heater pulse.

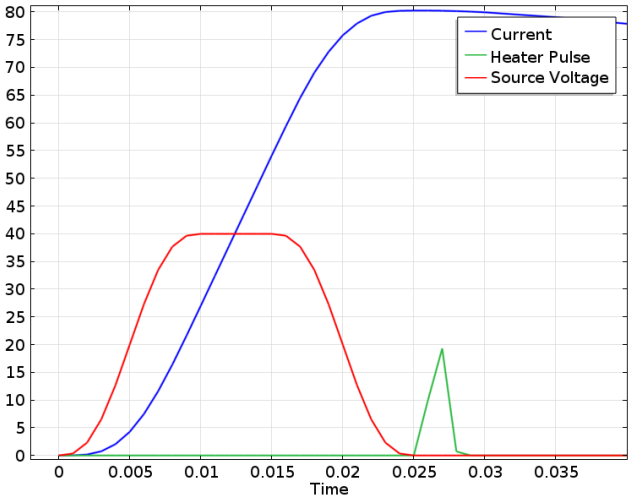

Fig. 24. Excitation of the circuit current by the voltage pulse and initiation of the quench.

Fig. 25 shows temperature distribution inside the coil at the moment t = 26 ms (immediately after the heat pulse is applied).

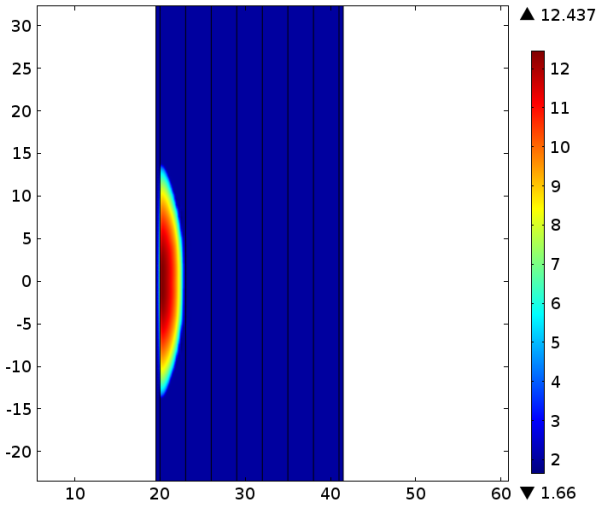

Fig. 25. Temperature in the coil at the moment t = 26 ms

In this case there is no need to use a special differential equation to describe the current in the circuit – it is calculated automatically through the multi-turn coil interface of the magnetic field node of the AC/DC module. We need just to supply right value of conductivity which depends on the temperature and magnetic field, as was done in the equation-based case (see expressions /7/ and /8/ earlier in this note). Main results of this part of the study are presented below. They should be compared with corresponding graphs from the previous chapter. Definitely we expect results similar to what was obtained earlier; while comparing the graphs, one should take into account the difference in the moments when the quench starts in both cases.

Fig. 26 shows the current in the circuit; it must be compared with Fig. 17.

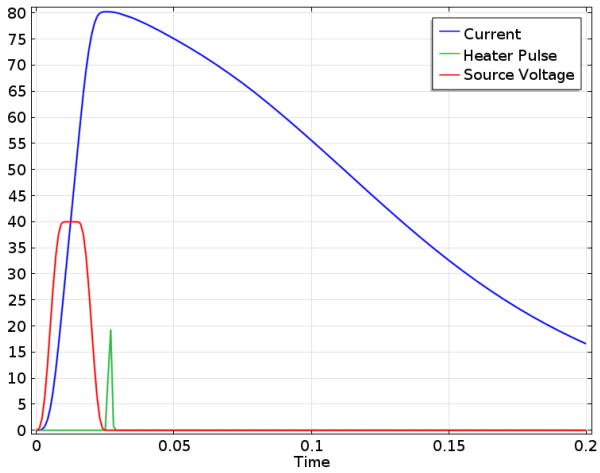

Fig. 26. Current in the discharge circuit

Quench starts after the heater is activated at t = 25 ms.

In Fig. 27, the temperature of the hottest spot is compared with that of the point with the maximum magnetic field. This graph must be compared with that in Fig. 18.

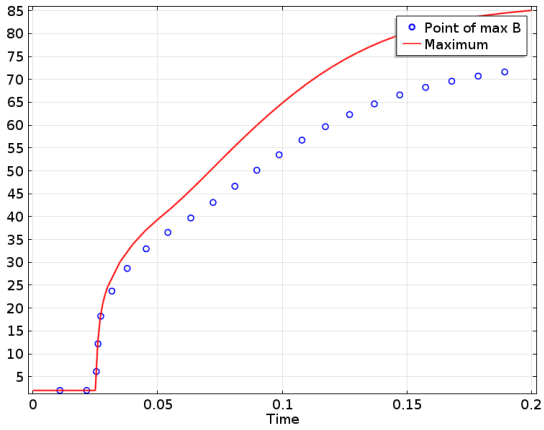

Fig. 27. Temperature in the coil

Resistances of the total coil and each of its sub-section are shown in Fig. 28, which must be compared with Fig. 19.

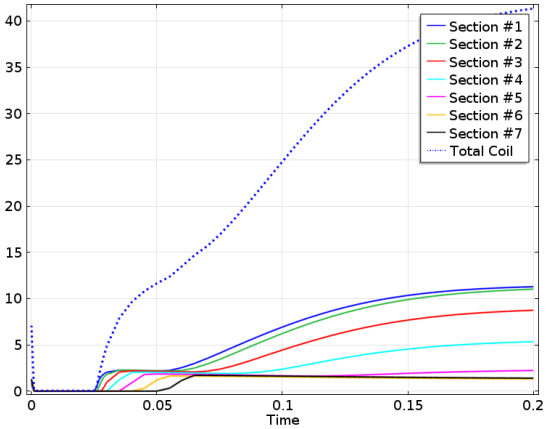

Fig. 28. Resistance of the coil and its sub-sections.

Heat deposition in the coil due to its resistivity is shown in Fig. 29; it should be compared with Fig. 20.

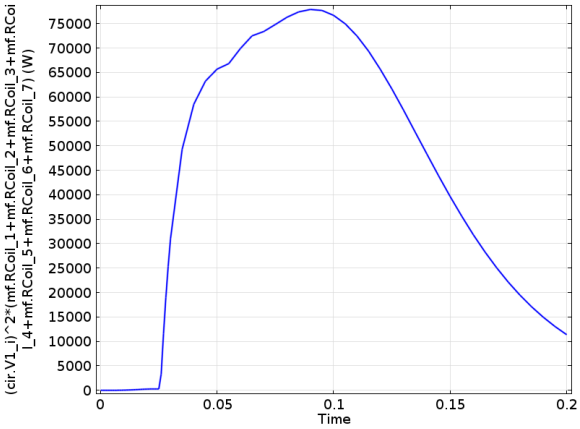

Fig. 29. Heating power $P = I^2 \cdot R$

Finally, voltages in the coil relative to the inner layer in Fig. 30 must be compared with similar graph for the equation-based case in Fig. 22.

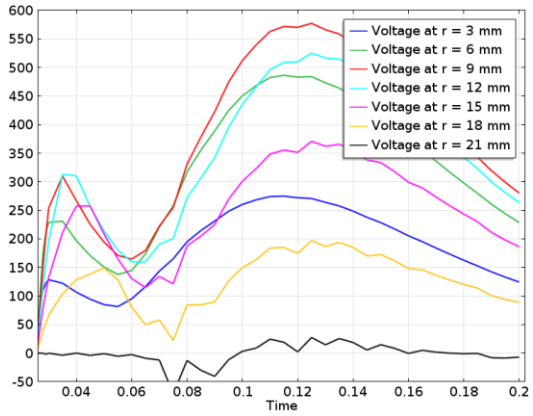

Fig. 30. Voltages inside the coil relative to the inner layer (r = 0)

Conclusion

In order to validate a new approach to modeling quench propagation in inductively coupled superconducting systems, two ways of the analysis were compared, both made within COMSOL environment and applied to the same axially symmetric system: the first way employed the global differential equation interface and the second one used the circuit interface of the AC/DC module. As the results obtained using these two methods proved to be quite comparable, each of them can be employed for the quench propagation analysis. The second way allows analysis of complex inductively-connected systems. The circuit interface of COMSOL makes the process of reconfiguration of the protection circuit quite simple and straightforward procedure. As a first step towards further study, this new approach will be used to verify results of the quench protection study in [6] obtained earlier using MATLAB environment.

References:

1. S. Obraztsov, I. Terechkine, "A Tool for Modeling Quench Propagation and Related Protection Issues", TD-06-063, Dec. 07, 2006.
2. V. Veretennikov, I. Terechkine, "SS-1 Section Focusing Lens Quench Protection Study", FNAL note TD-07-020, Aug. 2007
3. I. Terechkine, "SS2 Focusing Solenoid Quench Protection Study", TD-09-016
4. E. Khabiboulline, I. Terechkine, "SSR2 Focusing Lens Quench Protection Study", FNAL note TD-11-006.
5. E. Khabiboulline, I. Terechkine, "Modeling Quench Propagation in Inductively Coupled System of Coils", FNAL note TD-11-011.
6. I. Terechkine, "Quench Protection of the PXIE SSR1 Focusing Lens", FNAL TD note TD-13-011, Oct. 2013.
7. E.D. Marquardt, J.P. Le, Ray Radebaugh (NIST, Boulder, CO), "Cryogenic Material Properties Database", 11-th International Cryocooler Conference, June 20 – 22, 2000, Keystone, CO
8. http://www.illinoisacceleratorinstitute.org/2011%20Program/student_papers/Andrew_Davies.pdf
9. L. Bottura, "A Practical Fit for the Critical Surface of NbTi", IEEE Trans. Appl. Supercond., v. 10, No. 1, March 2000.
10. http://www.oxford-instruments.com/products/superconducting-magnets-and-wire/superconducting-wire/nb-ti-copper-matrix-monolith?src=mn
11. K.-H. Mess, et al, Superconducting Accelerating Magnets, World Scientific Publishing, 1996, p. 32.
12. I. Terechkine, "Modeling Quench Propagation in Superconducting Cavity Using COMSOL", FNAL TD note TD-11-019, Dec. 2011.